The Journal of Neuroscience, July 1, 1996, *16*(13):4089–4101

The Role of K^+ Currents in Frequency-Dependent Spike Broadening in *Aplysia* R20 Neurons: A Dynamic-Clamp Analysis

Minghong Ma[1,3,4] **and John Koester**[1,2,4]

[1]*Center for Neurobiology and Behavior,* [2]*Department of Psychiatry, and* [3]*Department of Physiology and Cellular Biophysics, College of Physicians and Surgeons, Columbia University, and* [4]*The New York State Psychiatric Institute, New York, New York 10032*

The R20 neurons of *Aplysia* exhibit frequency-dependent spike broadening. Previously, we had used two-electrode voltage clamp to examine the mechanisms of this spike broadening (Ma and Koester, 1995). We identified three K^+ currents that mediate action-potential repolarization: a transient A-type K^+ current (I_{Adepol}), a delayed rectifier current ($I_{K\text{-}V}$), and a Ca^{2+}-sensitive K^+ current ($I_{K\text{-}Ca}$). A major constraint in that study was the lack of completely selective blockers for I_{Adepol} and $I_{K\text{-}V}$, resulting in an inability to assess directly the effects of their activation and inactivation on spike broadening. In the present study, the dynamic-clamp technique, which employs computer simulation to inject biologically realistic currents into a cell under current-clamp conditions (Sharp et al., 1993a,b), was used either to block I_{Adepol} or $I_{K\text{-}V}$ or to modify their inactivation properties.

The data in this paper, together with earlier results, lead to the following hypothesis for the mechanism of spike broadening in the R20 cells. As the spike train progresses, the primary responsibility for spike repolarization gradually shifts from I_{Adepol} to $I_{K\text{-}V}$ to $I_{K\text{-}Ca}$. This sequence can be explained on the basis of the relative rates of activation and inactivation of each current with respect to the constantly changing spike durations, the cumulative inactivation of I_{Adepol} and $I_{K\text{-}V}$, and the progressive potentiation of $I_{K\text{-}Ca}$. Positive feedback interactions between spike broadening and inactivation contribute to the cumulative inactivation of both I_{Adepol} and $I_{K\text{-}V}$. The data also illustrate that when two or more currents have similar driving forces and partially overlapping activation characteristics, selectively blocking one current under current-clamp conditions can lead to a significant underestimate of its normal physiological importance.

Key words: spike broadening; dynamic clamp; K^+ current; I_{Adepol}; inactivation; Aplysia; *R20*

Frequency-dependent spike broadening, an endogenously generated increase in spike duration that increases as a function of firing rate, has been shown in neurons from a variety of species to be correlated with enhanced transmitter release (Gillette et al., 1980; Coates and Bulloch, 1985) and to result primarily from inactivation of K^+ currents (Aldrich et al., 1979a,b; Jackson et al., 1991; Bielefeldt et al., 1992; Crest and Gola, 1993; Quattrocki et al., 1994). Previously we had described the facilitatory synaptic effects and the mechanisms of frequency-dependent spike broadening in the two electrically coupled peptidergic R20 neurons of *Aplysia* (Ma and Koester, 1995). In addition, to analyze the mechanisms underlying spike broadening, several voltage-activated currents were isolated from the R20 cells by conventional voltage-clamp methods. These included a Na^+ current (I_{Na}), a multi-component Ca^{2+} current (I_{Ca}), and three K^+ currents—a high-threshold transient A-type current (I_{Adepol}), a delayed rectifier current ($I_{K\text{-}V}$), and a two component Ca^{2+}-sensitive K^+ current ($I_{K\text{-}Ca}$). By using a tape-recorded train of broadening spikes as the command signal for the voltage clamp, we found that I_{Adepol}, which is the largest outward current during a single nonbroadened spike, undergoes cumulative inactivation during such a train; $I_{K\text{-}V}$ exhibits bimodal changes, increasing during the early part of a train and decreasing during the latter part; $I_{K\text{-}Ca}$ facilitates throughout the train; and although the amplitude of I_{Ca} decreases during the train, its time integral increases. We hypothesized that the inactivation of I_{Adepol} is the motive force driving spike broadening in the R20 cells and that most changes in the other currents occur secondary to increasing spike width (Ma and Koester, 1995). We further postulated that $I_{K\text{-}V}$ affects primarily the kinetics of broadening, whereas $I_{K\text{-}Ca}$ affects both the rate and extent of broadening. The goals of this study were to test directly the hypothesized roles of these three K^+ currents in spike broadening in the R20 cells and to determine how their relative rates of activation and inactivation affect the voltage-mediated interactions between them.

Four complementary methods have been developed to study the role of voltage-gated membrane conductances in shaping the electrical activity patterns of a neuron. One approach, to block individual currents pharmacologically (Byrne et al., 1979; Schwindt, 1992; Tierney and Harris-Warrick, 1992), often is limited by a lack of specific blockers. For example, in the R20 cells, no known blockers are completely selective for I_{Adepol} or $I_{K\text{-}V}$. A second approach is to simulate the electrical activity of the cell by using mathematical descriptions of all of its voltage-gated membrane conductances. Then, individual conductances can be modified during the simulation (Byrne, 1980a,b; Golowasch et al., 1992; De Schutter and Bower, 1994). A drawback to this method is the possible difficulty in obtaining accurate descriptions of several voltage-sensitive conductances. A third approach is to

Received March 1, 1996; revised April 16, 1996; accepted April 18, 1996.

This work was supported by National Institutes of Health Grant NS14385.

We thank Drs. I. Kupfermann, A. MacDermott, and S. Siegelbaum for comments on this manuscript.

Correspondence should be addressed to Dr. John Koester, Center for Neurobiology and Behavior, New York State Psychiatric Institute, 722 West 168th Street, New York, NY 10032.

express artificially the channel in a neuron in which it does not normally appear (Kaang et al., 1992) and then to observe the resultant changes in excitability properties. This approach is quite demanding technically. Moreover, as our results confirm, the functional role of a voltage-gated conductance is highly dependent on the other types of voltage-gated conductances in the neuron, because of interactions via changes in membrane potential (McCormick and Huguenard, 1992; Ducreux and Puizillout, 1995). A fourth method is the dynamic-clamp technique.

The dynamic clamp uses computer simulation to introduce, eliminate, or modify voltage-gated conductances in biological neurons (Sharp et al., 1993a,b). The resultant changes in excitability then provide a direct readout of the role of the simulated conductance. This method has the advantage over the standard simulation method (above) that only the specific current being simulated needs to be accurately modeled. The remaining currents are calculated and generated automatically by the membrane. The kinetics, voltage sensitivity, or ion selectivity of the conductance can be modified, and the resultant effects on excitability can be determined.

In this study we used the dynamic clamp to block I_{Adepol} and/or $I_{\text{K-V}}$ or to modify their inactivation in the R20 neurons. The resultant changes in spike broadening can be explained by considering the kinetics of I_{Adepol}, $I_{\text{K-V}}$, and $I_{\text{K-Ca}}$ and the complex set of interactions among them that are mediated via changes in action-potential shape.

MATERIALS AND METHODS

Preparations. Aplysia californica (100–250 gm) were supplied by Marinus (Long Beach, CA). Each animal was anesthetized by the injection of isotonic $MgCl_2$, and the abdominal ganglion was dissected out and desheathed after being bathed in artificial sea water (ASW) containing 0.5% glutaraldehyde for 45 sec to reduce spontaneous contractions of the sheath muscle. The R20 cells were identified as described previously (Alevizos et al., 1989). The main axon branches of the R20 cells were truncated by cutting short the branchial nerve and the commissure between the two hemiganglia to improve the space clamp of the R20 somata. Then the ganglion was allowed to recover for at least 1 hr before each experiment, which was performed at 15 ± 1°C.

Pharmacology. The following compounds were used: tetrodotoxin (TTX) (Calbiochem, San Diego, CA); Tris (pH 7.6), $CdCl_2$, 4-aminopyridine (4-AP), and tetraethylammonium (TEA) (Sigma Chemical, St. Louis, MO). Each pharmacological blocker was applied by injecting a 100-fold concentrated bolus into the recording chamber directly by pipette. The composition of ASW was as follows (in mM): 460 NaCl, 10 KCl, 11 $CaCl_2$, 55 $MgCl_2$, 2.5 $NaHCO_3$, and 10 Tris.

The various ionic currents isolated as difference currents were I_{Na} (blocked by 60 μM TTX), total I_{Ca} (blocked by 2 mM $CdCl_2$ after I_{Na} and all K^+ currents had been blocked), I_{Adepol} (blocked by 1 mM 4-AP after $I_{\text{K-V}}$ and $I_{\text{K-Ca}}$ had been blocked), $I_{\text{K-V}}$ (blocked by 40 mM TEA after $I_{\text{K-Ca}}$ had been blocked), and $I_{\text{K-Ca}}$ (blocked by 3–4 mM TEA). See Ma and Koester (1995) for a discussion of the selectivity of these drugs on the R20 cells.

Voltage clamp. Standard two-electrode voltage-clamp and current-clamp methods were implemented using an Axon Instruments Axoclamp 2A (Foster City, CA), as described previously (Ma and Koester, 1995). In voltage-clamp mode, rectangular voltage steps combined with pharmacological blockers were used to identify I_{Adepol} and $I_{\text{K-V}}$ conductances in the R20 cells and to determine the parameters for simulating them with the dynamic clamp.

In some experiments, tape-recorded action-potential trains were played back as commands for the voltage clamp in order to determine directly how individual currents change during action-potential trains (for details, see Ma and Koester, 1995). In short, a train of gradually broadening action potentials evoked by injecting brief current pulses into the soma of an R20 cell was tape-recorded under current clamp in normal ASW. Then, with the same cell voltage-clamped, the action-potential train was played back as the command signal for the voltage clamp. When the command was repeated before (control) and after adding a specific channel blocker to the bath, the difference currents obtained by subtracting the currents with blocker from the control currents gave the waveforms of the specific currents that contributed to action-potential generation in current-clamp mode. The action-potential trains were 7 Hz for ~10 sec in all experiments. Every other spike and its corresponding current waveform are plotted in each figure where data from spike trains are presented. Duration of an action potential was defined as the time from the peak to the midpoint of its falling phase. All group data are expressed as mean ± SEM.

Empirical determination of I_{Adepol} *and* $I_{K\text{-}V}$. Both I_{Adepol} and $I_{\text{K-V}}$ were simulated by the dynamic clamp using standard Hodgkin–Huxley-type equations (Hodgkin and Huxley, 1952) of the form:

$$I_x = G_{\max} m^4 h (V_m - E_{\text{rev}}) \quad (1)$$

$$m(t + \Delta t) = m_\infty - (m_\infty - m(t))\exp(-\Delta t/\tau_m) \quad (2)$$

$$h(t + \Delta t) = h_\infty - (h_\infty - h(t))\exp(-\Delta t/\tau_h), \quad (3)$$

in which $G_{\max}$ is the conductance when all channels of type x are open, E_{rev} is the reversal potential for I_x, m_∞ and h_∞ are the steady-state values of the activation and inactivation variables at a given potential, Δt is the time step used in the integration, and t is the time at the end of the last integration step. The time constants τ_m and τ_h and steady-state values m_∞ and h_∞ at different voltage levels were obtained by conventional voltage-clamp protocols. In short, I_x (obtained as a pharmacological difference current) was activated by a series of depolarizing steps, the rising phases of the current were fit with fourth-power exponential functions to calculate the activation time constant (τ_m), and the decay phases were fit with single exponential functions to give the inactivation time constants (τ_h). (Deviations of I_{Adepol} or $I_{\text{K-V}}$ from typical Hodgkin–Huxley kinetics and the resultant approximations introduced into our model are described in Results.) For voltage steps that were too negative to activate I_x, the deactivation time constants (τ_m) were determined by tail-current analysis. This protocol also gave the reversal potential for I_x and revealed a linear relationship between the instantaneous tail currents and voltage in the range from −50 to +50 mV for both I_{Adepol} and $I_{\text{K-V}}$. The time constants for recovery from inactivation (τ_h) were determined by a two-pulse protocol (see inset in Fig. 3*A*). The maximum activation of the conductance underlying I_x ($G_{\max}$) and the voltage dependence of the activation variable (m_∞) were examined by plotting peak conductance (G_p) versus membrane potential. G_p was calculated as: $G_p = I_{\text{peak}}/(V_m - E_{\text{rev}})$, in which I_{peak} was measured by extrapolating the exponential decay of I_x to $t = 0$, the start of the pulse. The resulting conductances (G_p) and the voltages (V_m) were fit to a Boltzmann function of the form: $G_p = G_{\max}/1 + \exp((V_m - V_{1/2})/k)$, to estimate the maximum conductance, in which $V_{1/2}$ is the potential when G_p becomes half of $G_{\max}$ and k is the slope factor of the curve. The value of m_∞ at each membrane potential was calculated from equation 1 by setting h to its value at $t = 0$ and substituting I_{peak} for I_x. The voltage dependence of steady-state inactivation of I_x (h_∞) was estimated by a two-pulse protocol: a 100 msec test pulse to +30 mV was preceded by 2 sec pulses to a prepulse potential, which on different trials ranged from −80 to 0 mV. The value of G_p during each test pulse, normalized to its value after a −80 mV-conditioning pulse, was plotted against the corresponding prepulse potential and fitted to a Boltzmann function, which described the curve of h_∞ versus voltage.

The rate factors of α_m (activation), β_m (deactivation), α_h (recovery from inactivation), and β_h (inactivation) at each value of membrane potential were calculated from time constants of activation and inactivation and steady-state value of m and h, according to: $\alpha_m = m_\infty/\tau_m$, $\beta_m = (1 - m_\infty)/\tau_m$, $\alpha_h = h_\infty/\tau_h$, and $\beta_h = (1 - h_\infty)/\tau_h$. Then α_m, β_m, α_h, and β_h were fit by appropriate versions of the expression $(a + bV)/c + \exp((d + V)/f)$, with a, b, c, d, and f as adjustable parameters that were used to represent the different rate factors in the dynamic-clamp program. The dynamic-clamp software computed the current flow through each type of channel by integrating equations 2 and 3 and plugging the outputs into equation 1.

Dynamic clamp protocols. The setup for dynamic clamping is illustrated in Figure 1 (Sharp et al., 1993a,b). Dclamp 2.0 simulation software (Dyna-Quest Technologies, Sudbury, MA) running on a Tangent 486, 33 MHz computer connected to the preparation via a TL-1 DMA interface (Axon Instruments) was used to simulate either I_{Adepol} or $I_{\text{K-V}}$. The sampling rate for simulating a single conductance by dynamic clamp was 5 kHz. Parameters for the Hodgkin–Huxley-type equations describing the time and voltage dependence of the I_{Adepol} and $I_{\text{K-V}}$ conductances, which

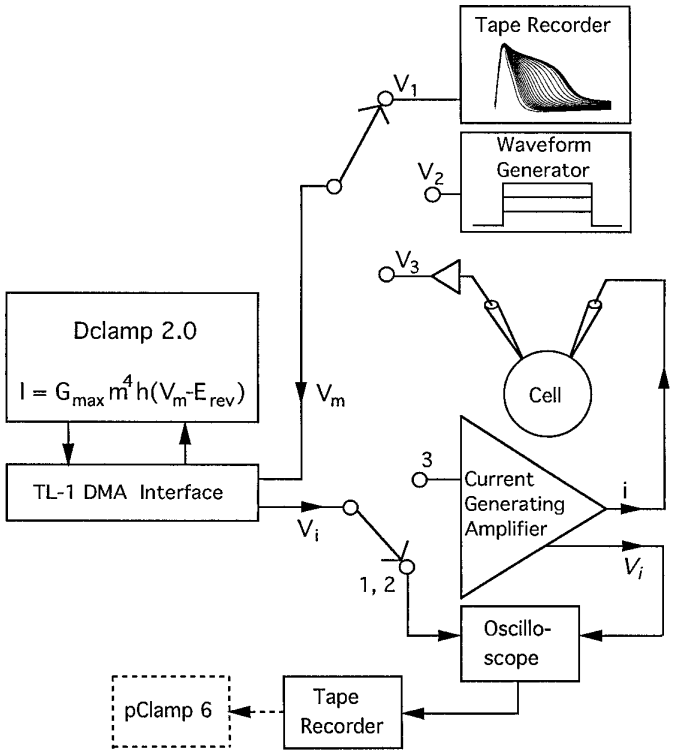

Figure 1. The dynamic clamp was used in open-loop mode to simulate current waveforms off-line in response to predetermined voltage commands consisting of either (1) a train of recorded spike waveforms, (2) rectangular voltage steps, or (3) in closed-loop mode to inject, block, or modify currents on-line.

had been determined empirically in other R20 cells, were entered into the dynamic-clamp program. Any one of three kinds of membrane potential signal (V_m) could be used as input to the dynamic-clamp program: an (off-line) tape-recorded action-potential train (V_1), a rectangular voltage step from a waveform generator (V_2), or membrane potential recorded from the neuron on-line (V_3). On the basis of the V_m signal and equations 1–3 (above) describing the desired conductance, the current i (I_{Adepol} or $I_{K\text{-}V}$) flowing through the conductance was computed by the dynamic clamp and expressed as a voltage signal (V_i) proportional to i. In open-loop mode (position 1 or 2), the dynamic clamp was used simply to calculate off-line the current flowing in response to a series of voltage steps or during a spike train. For these simulations, V_i was tape recorded for later playback and analysis. In closed-loop (on-line) mode (position 3), when the dynamic clamp was used to inject current (i) into the cell, V_i was used to control the injected current by driving the current-generating amplifier of the Axoclamp, and V_i, a signal proportional to i, was tape recorded for later playback and analysis. All voltage and current data were recorded on a modified VCR (PCM Data Recorder; A. R. Vetter, Rebersburg, PA) (sampling rate 22 kHz per channel) and on a Gould Brush 2400 chart recorder. The data played back from the tape recorder were analyzed by pClamp 6.0 software (Axon Instruments), which sampled the analog output of the tape recorder at 10 kHz per channel. All the current traces were filtered at 500 Hz by an RC software filter in pClamp 6.0. Output from the pClamp software was printed on a laser printer.

To block endogenous I_{Adepol} (or $I_{K\text{-}V}$) in the R20 cells, the dynamic clamp computed I_{Adepol} (or $I_{K\text{-}V}$) with reversed polarity and injected it into the cell. To block the inactivation of I_{Adepol} (or $I_{K\text{-}V}$), two currents were injected simultaneously: one was reversed I_{Adepol} (or $I_{K\text{-}V}$) to block the endogenous I_{Adepol} (or $I_{K\text{-}V}$) through the membrane, and the other was I_{Adepol} (or $I_{K\text{-}V}$) with normal polarity but with the h inactivation variable fixed at a value of 1.0.

The kinetic parameters for the dynamic-clamp equations describing the voltage- and time-dependent behavior of $I_{K\text{-}V}$ and I_{Adepol} were determined from group data obtained in separate experiments, but G_{max} for each of the two currents varied significantly between cells. Therefore, we did not use G_{max} values averaged from several cells to calculate G_{max} for a given experiment in which the K^+ current of an R20 cell was modified on-line by the dynamic clamp. Rather, in each such experiment, several values of G_{max} were used for a given protocol. These steps bracketed the average value from group data for each current (1700 nS for I_{Adepol}, 2100 nS for $I_{K\text{-}V}$) in steps of ± 10%. Then, at the end of the experiment, we measured G_{max} for each current directly. G_{max} was determined by measuring 40 mM TEA difference currents for $I_{K\text{-}V}$ and 1 mM 4-AP difference currents for I_{Adepol} for large depolarizing steps that maximally activated each conductance. In this procedure, I_{Na}, I_{Ca}, and $I_{K\text{-}Ca}$ were preblocked by 60 μM TTX and 2 mM $CdCl_2$ to improve space clamp and to eliminate the nonspecific effects of TEA and 4-AP on $I_{K\text{-}Ca}$ (see below). The data for the dynamic-clamp run in which G_{max} most closely matched the G_{max} value measured at the end of the experiment were chosen for further analysis. The one exception to this protocol was an experiment in which $I_{K\text{-}V}$, I_{Adepol}, and $I_{K\text{-}Ca}$ were blocked at the start of the experiment with 50 mM TEA and 10 mM 4-AP (see Fig. 10). In this experiment, G_{max} for I_{Adepol} was adjusted such that the first spike duration matched that of the control. Then G_{max} for $I_{K\text{-}V}$ was adjusted such that broadening with I_{Adepol} and $I_{K\text{-}V}$ added back roughly matched the broadening pattern seen when $I_{K\text{-}Ca}$ was blocked pharmacologically (see Fig. 14 in Ma and Koester, 1995).

In experiments in which conductances were added to a cell, the results were relatively insensitive to the value of G_{max} chosen, with values that varied by as much as ±50% in some cases providing qualitatively similar results. Blocking a conductance with the dynamic clamp was much more sensitive to the value of G_{max} chosen, however, as inadvertent overblock of either of the K^+ conductances resulted in a negative-slope conductance that destabilized the cell (Sharp et al., 1993b).

RESULTS

Voltage-clamp data revealed changing current waveforms correlated with spike broadening

R20 cells undergo an unusually high degree of frequency-dependent spike broadening. When fired in a train of 60 spikes at fixed frequencies ranging from 1 to 10 Hz, the duration of the action potentials in R20 neurons increases in a range from two-fold, at 1 Hz, to a maximum broadening of 5- to 10-fold in the range of 4–8 Hz (Ma and Koester, 1995). In studying the mechanisms of spike broadening in the R20 cells, we previously had combined conventional voltage-clamp techniques with various channel blockers to isolate five major ionic currents. Figure 2 illustrates the results obtained by using a tape-recorded train of broadening action potentials as the command signal for the voltage-clamp circuit for generating various pharmacological difference currents, as described in Materials and Methods (see also Ma and Koester, 1995). I_{Na} inactivated only slightly during a spike train and did not contribute to spike broadening directly. The peaks of I_{Ca} showed modest inactivation, but the duration of Ca^{2+} influx increased throughout the train, causing the time integrals of I_{Ca} to facilitate by about 2.5- to 4.0-fold. The prolonged I_{Ca} maintained the shoulders of the broadened spikes. I_{Adepol}, which was the largest outward current during a single nonbroadened spike, underwent steadily increasing inactivation during such a train. This cumulative inactivation was postulated to be the critical factor leading to spike broadening. $I_{K\text{-}V}$ exhibited bimodal changes that were proposed to influence the kinetics of spike broadening in two ways: $I_{K\text{-}V}$ increased during the early part of a train, slowing spike broadening, and decreased during the latter part, thereby accelerating broadening. The time integrals of $I_{K\text{-}Ca}$ facilitated throughout the train, opposing spike broadening. This increased $I_{K\text{-}Ca}$, along with the gradual inactivation of I_{Ca}, limited the maximal extent of broadening.

Although these experiments allowed us to determine how various currents change during a spike train, we were not able to use conventional methods to block all of the currents individually and determine the resulting effects on spike shape. Although selective blockers exist for $I_{K\text{-}Ca}$ (BAPTA or EGTA injection or low-dose

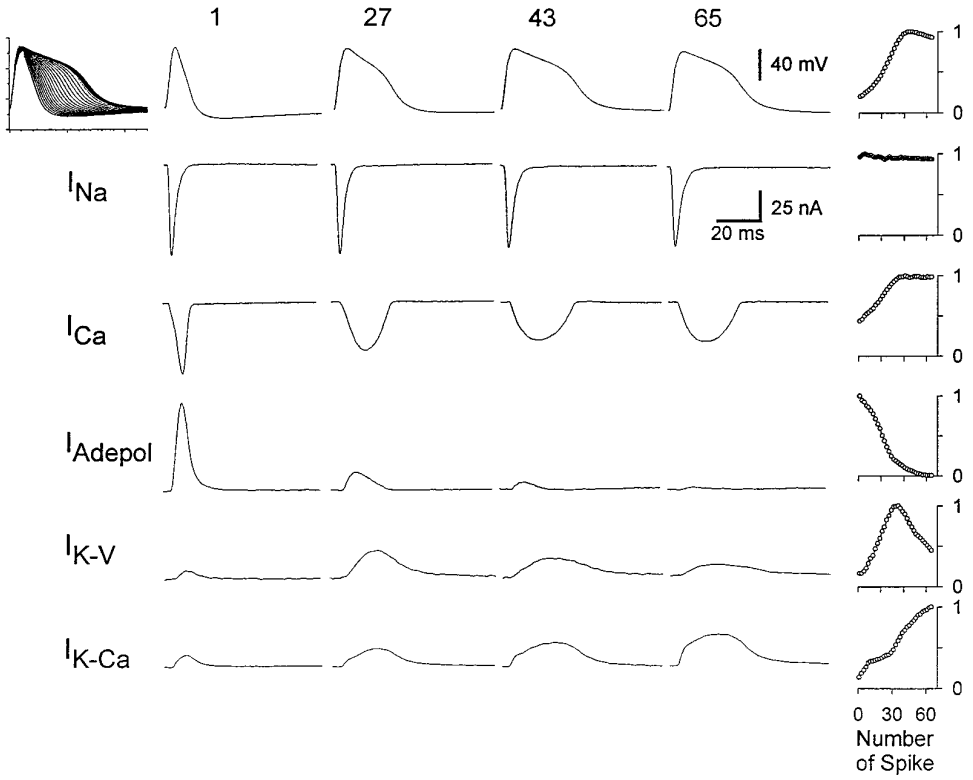

Figure 2. Characteristic patterns of changes in individual currents accompany frequency-dependent spike broadening. A 7 Hz, 9.3 sec action-potential train (*left, first row*) was evoked by injecting brief, depolarizing current pulses into a cell with a resting potential of −48 mV. The five major ionic currents mediating the spike train were isolated by playing back the spike train as the command to the conventional voltage clamp. Between each repetition of the train, the following sequence of blocking drugs was added, one at a time, to the bath: 60 μM TTX, 3 mM TEA, 40 mM TEA, 1 mM 4-AP, or 2 mM $CdCl_2$. The resulting difference currents measured before and after adding each compound revealed I_{Na}, $I_{K\text{-}Ca}$, $I_{K\text{-}V}$, I_{Adepol}, and I_{Ca}, respectively. The five major currents during the first spike, the 27th spike (at which point $I_{K\text{-}V}$ reached its peak), the 43rd spike (at which point the maximum broadening was reached), and the last spike (65th) are shown. The normalized values of spike duration and of the time integrals of each current are plotted against spike number in the right-hand column.

external TEA), the other outward currents (I_{Adepol} and $I_{K\text{-}V}$) could not be blocked in isolation because of the side effects of the available blockers. However, both I_{Adepol} and $I_{K\text{-}V}$ could be blocked specifically by a certain drug if the other currents affected by that compound had been preblocked by another compound. We used the following protocol to measure the voltage sensitivity and kinetics of each current. I_{Adepol} was measured as a 1 mM 4-AP difference current. Because 1 mM 4-AP also can increase a slow, outward current in the R20 cells, which appears to be $I_{K\text{-}Ca}$ (Ma and Koester, 1995), we preblocked $I_{K\text{-}Ca}$ and $I_{K\text{-}V}$ by adding 2 mM $CdCl_2$ (to block I_{Ca}) and 40 mM TEA before measuring the baseline current. Likewise, $I_{K\text{-}V}$ was isolated as a 40 mM TEA difference current. Because 40 mM TEA also blocks $I_{K\text{-}Ca}$, we again had to preblock $I_{K\text{-}Ca}$ by adding 2 mM $CdCl_2$. Descriptions of the reversal potentials, kinetics, and voltage sensitivities of the I_{Adepol} and $I_{K\text{-}V}$ conductances measured in this way were programmed into the dynamic-clamp software, which was used in later experiments to add, subtract, or modify the I_{Adepol} and $I_{K\text{-}V}$ conductances in living R20 cells.

The dynamic clamp can simulate I_{Adepol}

The first step in implementing the dynamic-clamp protocol is to obtain voltage-clamp data that can be used to create a model to simulate the current in question. I_{Adepol} could be modeled accurately by the classical Hodgkin–Huxley-type equations (see Materials and Methods) with two minor deviations. First, the time course of inactivation varied somewhat across cells: in most cells, it was well fit by a single exponential, whereas, in others, a relatively minor component of the current decayed at a somewhat slower exponential rate. Because the dynamic-clamp software we used cannot simulate a current with more than one time constant of inactivation, the rate of decay of I_{Adepol} at each voltage step was approximated by a single exponential, with time constant τ_h, over the voltage range from −20 to +50 mV. Second, time course of recovery from inactivation at −50 mV was described best by a double exponential function (Fig. 3*A*; Furukawa et al., 1992); the major component of recovery had a time constant of 1.1 ± 0.2 sec, although there was a much smaller component that had a time constant of 19.5 ± 2.8 sec (n = 4). Again, only the faster time constant at each voltage was used to approximate the kinetics of inactivation of I_{Adepol} (Fig. 3*A*). The data from conventional voltage-clamp experiments gave the following results for I_{Adepol}: $E_{rev} = -73.0 \pm 1.7$ mV (n = 5); $G_{max} = 1700 \pm 250$ nS (n = 8); $\alpha_m = 300/(0.9 + \exp((-6 + V_m)/(-15)))$; $\beta_m = 300/(3 + \exp((50 + V_m)/12))$; $\alpha_h = 1.8/\exp((62 + V_m)/20)$; and $\beta_h = 8.5/(0.43 + \exp((20 + V_m)/(-5)))$; $V_{1/2} = -11.5$ and −34.0 mV for m^4 and h, respectively.

The accuracy of the mathematical model of I_{Adepol} was tested in two ways. First, it was used to simulate I_{Adepol} waveforms in response to 200 msec depolarizing steps from −40 to +30 mV from a holding potential of −50 mV. The results were quite similar to the I_{Adepol} waveforms recorded as 1 mM 4-AP difference currents (Fig. 3*B1,B2*). Second, the values of I_{Adepol} during an action-potential train were simulated. The simulated currents were similar, but not identical, to those isolated pharmacologically. Although the calculated I_{Adepol} underwent cumulative inactivation similar to that shown by 1 mM 4-AP difference currents measured during a train of broadening spikes (Fig. 3*C1*), the final extent of inactivation of simulated I_{Adepol} at the end of the train was a bit less than that for the empirically measured I_{Adepol} (Fig. 3*C2,C3*). The reason was presumed to be that I_{Adepol} was simulated with only the fast-time constant for recovery from inactivation instead of two time constants, a fast one as well as a slow one (Fig. 3*A*). The lack of a major discrepancy between recorded and simulated currents suggests that the fast recovery process ac-

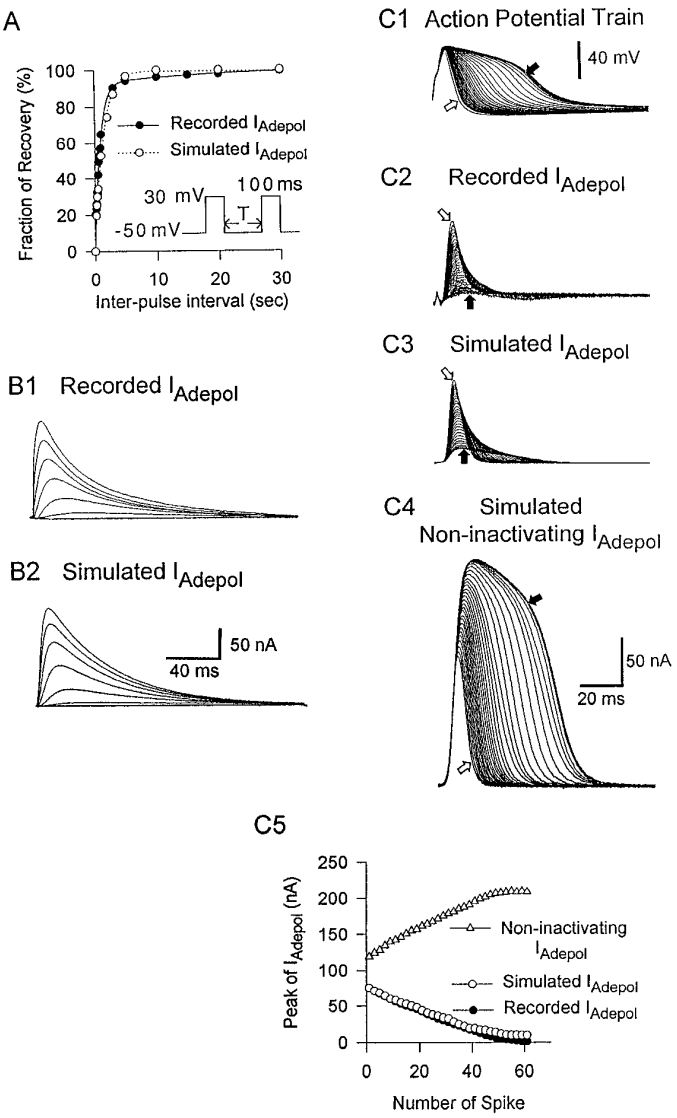

Figure 3. A mathematical model, which accurately simulates I_{Adepol}, illustrates the role of cumulative inactivation in the evolution of I_{Adepol} traces during a spike train. *A*, The recovery from inactivation of recorded I_{Adepol} has two time constants. A two-pulse protocol (*inset*) was used to determine the recovery from inactivation caused by the first 100 msec pulse from −50 to +30 mV. The peak current during the second pulse, normalized to that during the first one (*filled circles*), was plotted against the time interval between the two pulses. The curve (*smooth line*) was fit by a double exponential function; the major component had a τ_h value of 0.9 sec, whereas τ_h for the minor component was 18.5 sec. To simulate I_{Adepol}, the recovery from inactivation was approximated by using just the faster time constant, which was 1.1 sec at −50 mV, averaged from four experiments. The accuracy of this approximation was tested by using the same double-pulse protocol (*inset*) to drive the dynamic-clamp circuit in open-loop mode. The peak current calculated during the second pulse, normalized to that during the first pulse (*open circle*), was plotted against the time interval between two pulses, which was fit by a single exponential curve (*dotted line*). *B*, The model simulates I_{Adepol} during rectangular depolarizing steps. *B1*, Empirically measured I_{Adepol} in response to 200 msec depolarizing steps in 10 mV increments from −40 to +30 mV from a holding potential of −50 mV. *B2*, I_{Adepol} was simulated by driving the dynamic-clamp circuit in open-loop mode with the same set of depolarizing steps as those used in *B1*. *C*, The simulated I_{Adepol} traces during action-potential trains were quite similar to those recorded as 4-AP difference current. *C1*, An action-potential train evoked by injecting brief, depolarizing current pulses into the soma was recorded for use as a command signal. The holding potential was −40 mV. *C2*, I_{Adepol} was recorded as a 4-AP difference current under voltage clamp while playing back the spike train recorded in *C1*. *C3, C4*, I_{Adepol} was simulated by playing back the action-potential train from *C1* to the dynamic-clamp circuit in open-loop mode with two different versions of the model. *C3*, I_{Adepol} waveforms that were simulated with the unmodified version of the model matched the empirically determined values in *C2*. *C4*, When noninactivating I_{Adepol} was simulated by fixing $h = 1$, the same command led to greatly enhanced values of I_{Adepol}. *C5*, Changes in peak values of recorded and simulated I_{Adepol} from *C2–C4* are plotted against spike number. I_{Adepol} was measured as a 1 mM 4-AP difference current after 60 μM TTX, 2 mM $CdCl_2$, and 40 mM TEA had been added to block I_{Na}, $I_{K\text{-}Ca}$, and $I_{K\text{-}V}$. The value of G_{max} used in the simulations *C3*, *C4* was 1900 nS. The first and last *traces* in *C* are indicated by the *white* and *black arrows*, respectively.

counts for the bulk of the cumulative inactivation during a train, whereas the slow component plays a relatively minor role.

The importance of inactivation in shaping I_{Adepol} waveforms during a spike train was determined by blocking the inactivation of simulated I_{Adepol} currents while using the recorded spike train from Fig. 3*C1* as the input to the dynamic clamp. Blocking inactivation increases the peak of simulated I_{Adepol} during the first spike in the train by only 1.3-fold ± 0.1 ($n = 4$) (compare first traces in Fig. 3*C3* and *C4*), but as the train progresses and spike durations increase, the differences between the currents with or without inactivation increase dramatically. With inactivation intact, the gradual accumulation of I_{Adepol} channels in the inactivated state causes a progressive decrease in peak I_{Adepol} (Fig. 3*C3*). With inactivation blocked, peak I_{Adepol} increases during the train as the voltage command signals (spike waveforms) get longer and longer (Fig. 3*C4*). The maximum potentiation of I_{Adepol} caused by removing its inactivation reaches 27.0-fold (± 3.9; $n = 4$) at the end of the train (Fig. 3*C5*). This build-up of amplitude potentiation caused by removing inactivation occurs because the first spikes in the train are too brief to allow the I_{Adepol} activation variable to approach its steady-state value (m_∞) at the peak of the spike. This potentiation of modified (noninactivating) I_{Adepol} demonstrates that the degree of progressive inactivation that normally occurs for native I_{Adepol} during a train is even greater than one would conclude by simply observing the decline in I_{Adepol} peaks (Fig. 3*C5*).

The dynamic clamp can simulate $I_{K\text{-}V}$

The empirical determination of parameters describing the kinetics and voltage sensitivity of the $I_{K\text{-}V}$ channels was based on protocols similar to those described for I_{Adepol}, with one important exception. Brief depolarizing steps were found to be more effective in inactivating $I_{K\text{-}V}$ than was a long step of duration equivalent to that of the sum of the short steps (Fig. 4*A1,A2*). A similar phenomenon has been described previously for delayed rectifier currents in neurons of various species (Aldrich et al., 1979a,b; Marom and Levitan, 1994; Quattrocki et al., 1994; Baukrowitz and Yellen, 1995). The excess inactivation that results when a long depolarization is broken up into an equivalent train of short pulses is sometimes called "cumulative inactivation" (Aldrich, 1981). It is attributed to a state-dependent phenomenon, based on the coupling of activation and inactivation variables. (We use the term "cumulative inactivation" in a more generic sense to refer to any build-up in inactivation that occurs when repeated voltage pulses are applied, without implying a particular type of kinetic scheme.)

State-dependent coupling of activation and inactivation variables cannot be modeled by the classical Hodgkin–Huxley model encoded in the Dclamp 2.0 software. As a result, inactivation rates determined during a long depolarizing step cannot simulate accurately the kinetics of inactivation during a train of relatively

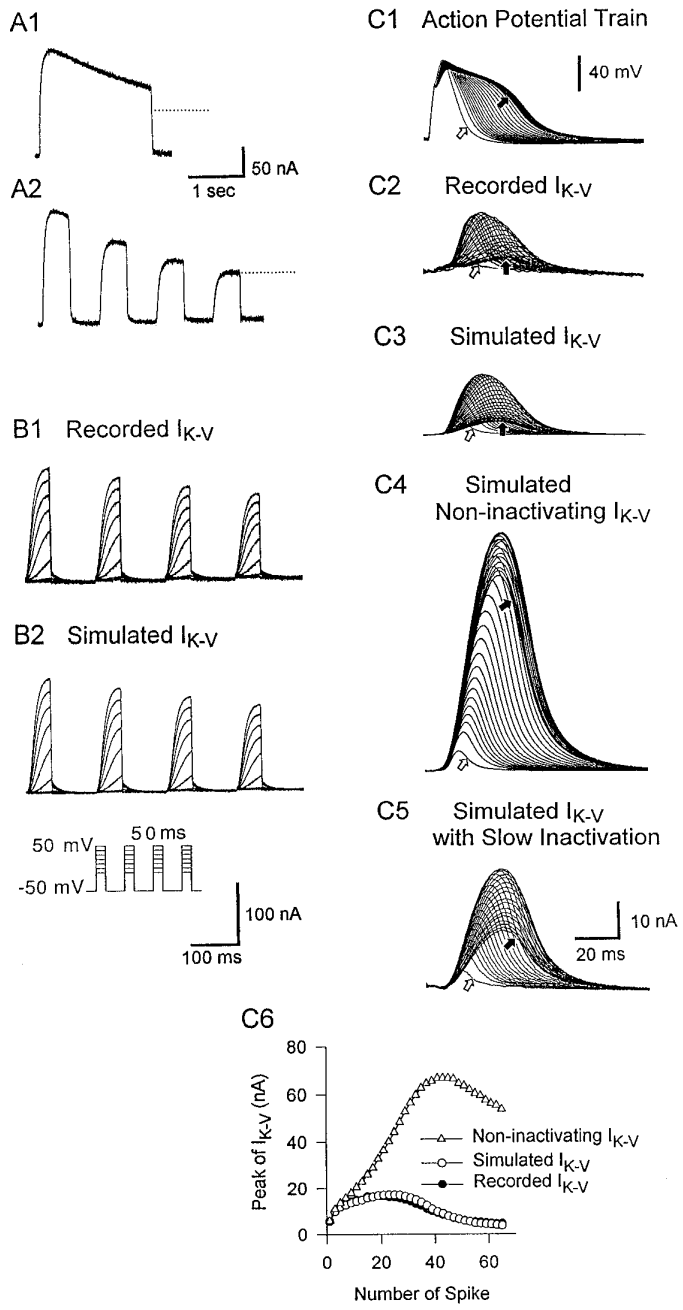

Figure 4. A mathematical model, which accurately simulates $I_{K\text{-}V}$, illustrates the role of cumulative inactivation in the evolution of $I_{K\text{-}V}$ traces during a spike train. *A*, $I_{K\text{-}V}$ exhibits state-dependent inactivation, which causes it to inactivate more rapidly in response to several brief pulses than to one long pulse of equivalent duration. Depolarizing steps were from a holding potential of −50 mV to +20 mV. *A1*, $I_{K\text{-}V}$ inactivated relatively slowly during a 2 sec depolarizing step. *A2*, $I_{K\text{-}V}$ during four 500 msec pulses repeated at 1 Hz decayed to a lower final level than in *A1*. The *dotted line* in *A1* marks the corresponding level of $I_{K\text{-}V}$ at the end of four brief voltage steps in *A2*. *B*, Recorded and simulated $I_{K\text{-}V}$ were similar during 50 msec repetitive depolarizing pulses (−10 to +50 mV) at 7 Hz from a holding potential of −50 mV. *B1*, $I_{K\text{-}V}$ was measured empirically as a TEA difference current using the voltage-step protocol shown in the inset. *B2*, $I_{K\text{-}V}$ was simulated by driving the dynamic-clamp circuit in open-loop mode. *C*, The simulated waveforms of $I_{K\text{-}V}$ during action-potential trains were similar to those recorded as TEA difference currents. *C1*, An action-potential train evoked by injecting brief depolarizing current pulses was recorded for use as a command signal. The holding potential was −50 mV. *C2*, $I_{K\text{-}V}$ was recorded as a TEA difference current under voltage clamp while playing back the spike train recorded in *C1*. *C3–C5*, $I_{K\text{-}V}$ was simulated by playing back the action-potential train from *C1* to the dynamic-clamp circuit in open-loop mode with three different versions of the model. *C3*, Simulated $I_{K\text{-}V}$ had normal inactivation. *C4*, Noninactivating $I_{K\text{-}V}$ was simulated by fixing $h = 1$. *C5*, The state-dependent nature of $I_{K\text{-}V}$ inactivation was ignored; τ_h was estimated from the decay during long (2 sec) voltage steps (*A1*) rather than from high-frequency trains of steps as in *B*. *C6*, Peak values of recorded and simulated $I_{K\text{-}V}$ from *C3–C5* are plotted against spike number. $I_{K\text{-}V}$ was measured as a 40 mM TEA difference current after 60 mM TTX and 2 mM $CdCl_2$ had been added to block I_{Na}, I_{Ca}, and $I_{K\text{-}Ca}$. The value of G_{max} used for the simulations in *C* was 1850 nS. The first and last traces in *C* are indicated by the *white* and *black arrows*, respectively.

brief action potentials. Instead, we used inactivation rates measured during a train of brief voltage steps (Fig. 4*B1*), which occurred at the same rate as the spikes in a train, to provide a Hodgkin–Huxley-type approximation of the state-dependent inactivation of $I_{K\text{-}V}$. In other words, the inactivation time constants of $I_{K\text{-}V}$ (τ_h) were not estimated from the decay of exponential curves during long pulses but were approximated by fitting the decay of the peak currents during a 7 Hz train of repeated 50 msec pulses (−10 to 50 mV) from a holding potential of −50 mV (inset of Fig. 4*B*). With this estimate of $I_{K\text{-}V}$ inactivation rates, the dynamic clamp could simulate rather accurately the empirically determined changes in $I_{K\text{-}V}$ during frequency-dependent spike broadening. This approach required sacrificing the accuracy of $I_{K\text{-}V}$ simulations during long voltage-clamp steps (>100 msec), which are not physiologically relevant in this case. With this modification in protocol, the kinetics and voltage sensitivity of the $I_{K\text{-}V}$ currents were fit by the equations described in Materials and Methods: $E_{rev} = -62.0 \pm 3.1$ mV ($n = 3$); $G_{max} = 2100 \pm 370$ nS ($n = 9$); $\alpha_m = (53 + 0.22\,V_m)/(0.65 + \exp((-5 + V_m)/(-13)))$; $\beta_m = (3.4 - 0.06V_m)/\exp((-10 + V_m)/65)$; $\alpha_h = 1/\exp((143 + V_m)/30)$; and $\beta_h = 1.7/(0.83 + \exp((7.4 + V_m)/(-7.7)))$; $V_{1/2} = 0.1$ and −33.0 mV for m^4 and h, respectively.

The accuracy of the mathematical model of $I_{K\text{-}V}$ was checked in two ways. First, the simulated waveforms of $I_{K\text{-}V}$ in response to four 7 Hz, 50-msec-depolarizing repetitive steps (−10 to +50 mV) from a holding potential of −50 mV were found to be quite similar to the values of $I_{K\text{-}V}$ measured empirically as 40 mM TEA difference currents (Fig. 4*B*). Second, the simulated $I_{K\text{-}V}$ waveforms during an action-potential train matched quite closely the waveforms measured empirically (Fig. 4*C1–C3*). The importance of using inactivation kinetics determined from high-frequency pulses (Fig. 4*B1*) was tested by trying an alternative kinetic model that used values of τ_h for $I_{K\text{-}V}$ that were determined by measuring the decay rate during a series of long (2 sec) voltage steps. When control action-potential waveforms were used to drive simulations based on such a conventional, nonstate-dependent model of $I_{K\text{-}V}$ inactivation, the computed $I_{K\text{-}V}$ waveforms deviated considerably from the empirically measured difference currents. The simulated currents showed much greater facilitation during the train, as well as a much lower level of inactivation at the end of the train (compare Fig. 4*C3* and *C5*).

The role of inactivation in shaping $I_{K\text{-}V}$ waveforms during a spike train was determined by modifying the inactivation of simulated $I_{K\text{-}V}$ currents while using the recorded spike train from Figure 4*C1* as the input to the dynamic clamp. Blocking inactivation has no significant effect on the simulated $I_{K\text{-}V}$ during the first spike in the train (compare Fig. 4*C3* to *C4*), but as the train progresses, the differences between the currents with or without inactivation rapidly increase. In both cases, as the spikes begin to

broaden during the train, peak $I_{K\text{-}V}$ increases as the spike waveforms get longer and longer, allowing the channels to approach more closely full activation. When inactivation is intact, however, this potentiating trend is overwhelmed rapidly by the gradual cumulative inactivation of $I_{K\text{-}V}$ channels, which causes a progressive decrease in peak $I_{K\text{-}V}$, beginning about a third of the way into the train (Fig. 4*C3*). In contrast, with inactivation blocked, peak $I_{K\text{-}V}$ increases throughout the train as the spike waveforms get longer and longer (Fig. 4*C4*). Only near the end of the train, as spike amplitude and duration decrease slightly because of potentiation of $I_{K\text{-}Ca}$ and inactivation of I_{Ca} (Ma and Koester, 1995), does $I_{K\text{-}V}$ begin to decrease slightly. The early onset of differences in $I_{K\text{-}V}$ patterns under the two conditions indicates that inactivation of $I_{K\text{-}V}$ plays an important role in shaping $I_{K\text{-}V}$ behavior even at the beginning of the control train, when $I_{K\text{-}V}$ is increasing from spike to spike. It also demonstrates that the degree of progressive inactivation of normally inactivating $I_{K\text{-}V}$ during a train is even greater than one would conclude simply by observing the decline in control $I_{K\text{-}V}$ peaks (Fig. 4*C6*). Blocking inactivation causes a much greater potentiation of $I_{K\text{-}V}$ than of I_{Adepol} in this protocol, because the rapid activation kinetics of I_{Adepol} allow it to approach much more closely full activation during the first spike of the train than does $I_{K\text{-}V}$, which activates relatively slowly. Potentiation measured as the ratio of the peak of the largest current trace to the peak of the first trace in the train was 10.6-fold ± 1.7 ($n = 4$) for $I_{K\text{-}V}$ but only 1.8 ± 0.4 ($n = 4$) for I_{Adepol} (compare Figs. 3*C5* to 4*C6*).

Both I_{Adepol} and $I_{K\text{-}V}$ control spike broadening

The dynamic clamp was used to study the effects of selectively blocking I_{Adepol} or $I_{K\text{-}V}$ on spike broadening and to study the effects of blocking the inactivation of either current both on spike broadening and on the dynamics of the other current. Pharmacological methods are not adequate for such manipulations, because the known blockers of the two types of ion channel are nonselective (Hermann and Gorman, 1981a,b; Ma and Koester, 1995), and there are no known pharmacological blockers of inactivation of these channels.

Blocking activation or inactivation of I_{Adepol} *modulates spike broadening*

Previously we had examined the roles of the three voltage-activated K^+ currents in spike repolarization (Ma and Koester, 1995). Our data showed that blocking both $I_{K\text{-}V}$ and $I_{K\text{-}Ca}$ with TEA so that I_{Adepol} was the only voltage-activated outward current remaining had no significant effect on the width of a single spike. When 1 mM 4-AP was added subsequently, it blocked I_{Adepol} selectively, because the previous addition of TEA had eliminated nonselective potentiation of $I_{K\text{-}Ca}$ from 4-AP. Under these conditions, pharmacological block of I_{Adepol} broadened a single spike by ~10-fold (Ma and Koester, 1995). These results suggested that, of the three outward currents, I_{Adepol} is the only one to affect significantly the repolarization rate for a single spike. Moreover, in the same study, cumulative inactivation of I_{Adepol} was found to correlate well with spike broadening during a high-frequency train (see also Figs. 2,3). One might expect, therefore, that selective block of I_{Adepol} would cause the first spike of a train to broaden to near its maximal value, but further broadening during the train would be negligible. In the present study, however, applying 1 mM 4-AP alone to block I_{Adepol} made a single spike only 2.2-fold (±0.2) wider and 9.6% (±1.3%) larger ($n = 8$), and major spike broadening still occurred later in the train (data not shown). Given that 4-AP also can facilitate $I_{K\text{-}Ca}$ (Hermann and Gorman, 1981a), the relatively minor effects of blocking I_{Adepol} on spike width could result from a countervailing enhancement of $I_{K\text{-}Ca}$. In fact, late in a train when $I_{K\text{-}Ca}$ reaches its peak value (Fig. 2 in Ma and Koester, 1995), broadening was more pronounced in controls than in cells treated with 4-AP (data not shown). These results suggest that 4-AP may indeed have potentiated $I_{K\text{-}Ca}$. To eliminate this possibility, we repeated this experiment by using the dynamic clamp, rather than 4-AP, to block I_{Adepol}. We found that selectively blocking I_{Adepol} with the dynamic clamp had results on a single spike similar to those produced by 4-AP—~two-fold broadening (Fig. 5*A1,A2*, 6*A*). Unlike 4-AP block, it showed no tendency to reduce broadening late in the train. We therefore restricted our analyses of the effect of blocking I_{Adepol} to experiments in which the dynamic clamp was used to cancel it out.

Given our earlier results on the importance of I_{Adepol}, why did blocking I_{Adepol} have such a small effect on initial spike width and subsequent broadening during a train (Figs. 5*A*, 6*A*)? One possibility is that $I_{K\text{-}V}$ and $I_{K\text{-}Ca}$, which normally activate relatively slowly, had sufficient time to activate more fully as a result of the twofold spike broadening caused by blocking I_{Adepol}. As a result of such increased activation, $I_{K\text{-}V}$ and $I_{K\text{-}Ca}$ could become the dominant outward currents underlying spike repolarization. In that case, cumulative inactivation of $I_{K\text{-}V}$ and a parallel decrease of $I_{K\text{-}Ca}$ could mediate the subsequent spike broadening. (Although the time integrals of $I_{K\text{-}Ca}$ increased overall during a spike train (Fig. 2), the peaks of $I_{K\text{-}Ca}$ did show a transient dip during the initial part of the train (Figs. 6*B1,B3*; Fig. 9 in Ma and Koester, 1995), perhaps because of the inactivation of Ca^{2+} channels nearest the $I_{K\text{-}Ca}$ channels.) This hypothesis for the enhanced role of $I_{K\text{-}V}$ and $I_{K\text{-}Ca}$ was tested by using two sets of action-potential trains, which had been recorded either under control conditions or while I_{Adepol} was blocked by the dynamic clamp. For $I_{K\text{-}V}$, these recorded spike trains were used as commands to the dynamic clamp, which simulated the $I_{K\text{-}V}$ waveforms off-line in response to the two different spike trains (Fig. 5). For $I_{K\text{-}Ca}$, the same recorded spike trains were used as commands to the voltage clamp, and 3 mM TEA was applied to isolate $I_{K\text{-}Ca}$ during the two different spike trains (Fig. 6). As predicted, (1) the simulated $I_{K\text{-}V}$ (Fig. 5*B*) and the measured $I_{K\text{-}Ca}$ (Fig. 6*B*) activated much more completely during the first spike compared with the first spike when I_{Adepol} was normal; (2) $I_{K\text{-}V}$ underwent cumulative inactivation during spike trains recorded when I_{Adepol} was blocked (Fig. 5*B2,B4*); and (3) peaks of $I_{K\text{-}Ca}$ decreased during the early part of the spike train, as though the initial transient dip were enhanced (Fig. 6*B2,B3*).

We had postulated that in control conditions inactivation of I_{Adepol} is critical for spike broadening, because I_{Adepol} is normally the largest outward current during a single spike and because its cumulative inactivation mirrors the increase in spike duration (see also Fig. 2; Ma and Koester, 1995). This hypothesis was supported by an experiment in which the inactivation of I_{Adepol} was blocked by the dynamic clamp. Under these conditions spike broadening was negligible ($n = 14$). As a result of spike width staying constant during such a train, the simulated peak values of $I_{K\text{-}V}$ did not facilitate. Instead, they exhibited only steadily increasing inactivation during a train of nonbroadened spikes (Fig. 5*A3,B3,B4*; see also below). Although the model used to simulate $I_{K\text{-}V}$ can only approximate its complex inactivation kinetics, similar results were obtained when $I_{K\text{-}V}$ was measured directly as a TEA difference current in a similar protocol (Fig. 12 in Ma and Koester, 1995).

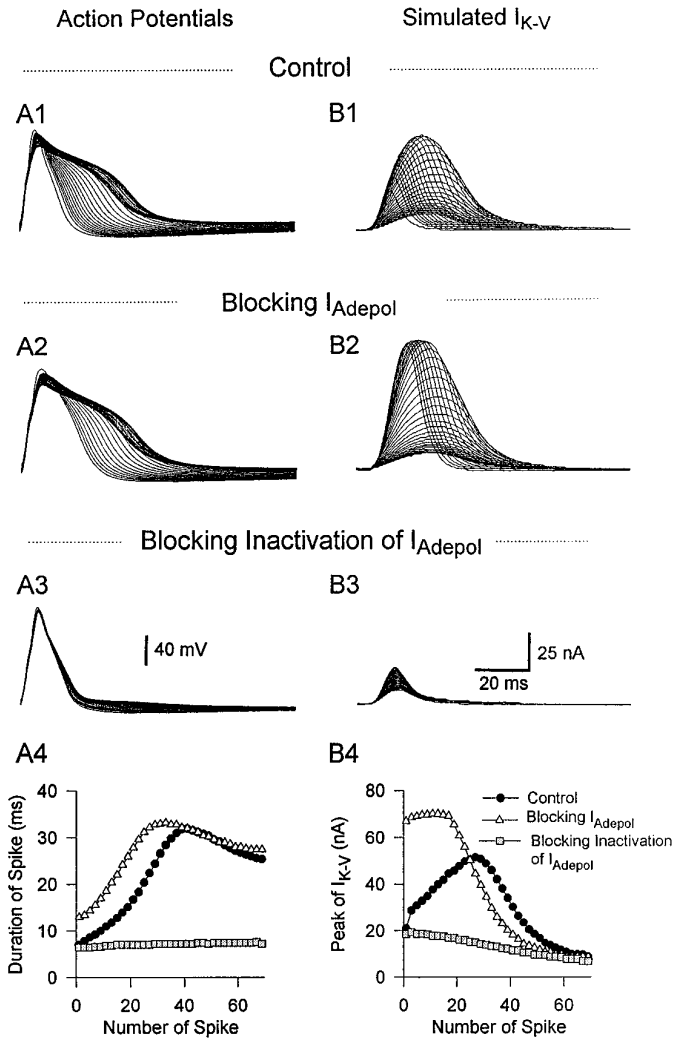

Figure 5. Blocking I_{Adepol} activation (or inactivation) with the dynamic clamp accelerated (or eliminated) spike broadening, which in turn modified the dynamics of I_{K-V} activation and inactivation. *A*, Action-potential trains were evoked under control conditions (*A1*), after blocking I_{Adepol} (*A2*), or after blocking inactivation of I_{Adepol} (*A3*). The dynamic clamp was used in closed-loop mode either to simply cancel out I_{Adepol} (*A2*) or to replace it with a noninactivating version of I_{Adepol} (*A3*). *B*, Simulated I_{K-V} changed during a spike train recorded while I_{Adepol} (or its inactivation) was blocked. *B1*, Simulated I_{K-V} during a control spike train showed bimodal changes. *B2*, Simulated I_{K-V} during an action-potential train recorded while I_{Adepol} was blocked underwent cumulative inactivation from the increased initial value. *B3*, Simulated I_{K-V} during a spike train recorded while inactivation of I_{Adepol} was blocked underwent only modest cumulative inactivation. *A4, B4*, Changes in spike width (*A1–A3*) and peak values of simulated I_{K-V} (*B1–B3*) caused by modifying I_{Adepol} are plotted against spike number. Resting potential was −50 mV. G_{max} used by the dynamic clamp for blocking or modifying I_{Adepol} was 1650 nS. G_{max} used for simulating I_{K-V} in *B1–B3* was 2050 nS.

An important positive feedback interaction between spike broadening and I_{K-V} inactivation was revealed by examining the simulated I_{K-V} currents under two different conditions. When I_{Adepol} inactivation was blocked, thereby preventing spike broadening, the simulated I_{K-V} currents reached a maximal cumulative inactivation of only ~50% (Fig. 5*B3*). When broadening was allowed to occur, I_{K-V} inactivated to ~12% of its maximum value earlier in the train (Fig. 5*B2*).

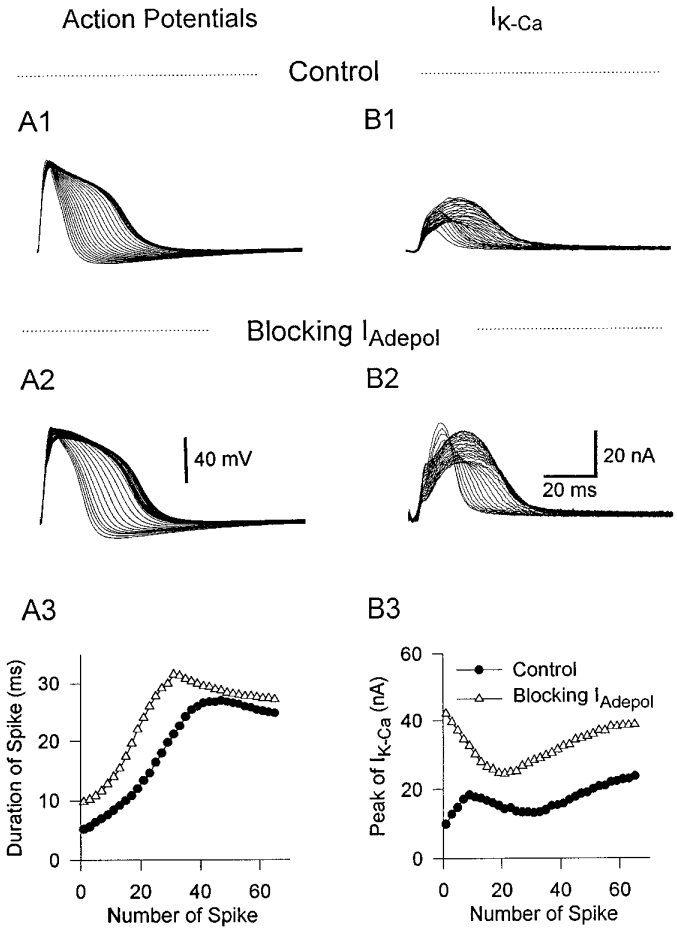

Figure 6. Blocking I_{Adepol} activation with the dynamic clamp accelerated spike broadening, which, in turn, enhanced the activation of I_{K-Ca} and modified its kinetics. *A*, The spike trains recorded either under control conditions (*A1*) or with I_{Adepol} activation blocked (*A2*) by the dynamic clamp were used as commands to the voltage clamp for isolating I_{K-Ca} pharmacologically (*B1, B2*). *B*, I_{K-Ca} was measured as 3 mM TEA difference currents under control condition (*B1*) and after blocking I_{Adepol} (*B2*). *A3, B3*, The durations of the spikes of the two trains (*A1, A2*) and the corresponding peaks of I_{K-Ca} currents (*B1, B2*) are plotted against spike number. Resting potential was −50 mV, and G_{max} used for the I_{Adepol} simulations (*A2*) was 1350 nS.

Blocking activation or inactivation of I_{K-V} *modulates spike broadening*

I_{K-V} normally starts out small for the first spike in the train and then increases, before eventually decreasing toward its initial value late in the train (see also Fig. 2; Ma and Koester, 1995). Thus, we predicted that blocking I_{K-V} with the dynamic clamp would have relatively little effect on the first or last spikes in the train but would increase the rate of broadening during the early and middle parts of the train, when I_{K-V} normally increases in amplitude. As expected, blocking I_{K-V} had negligible effects on the durations of the first and last spikes in the train, but it accelerated the process of spike broadening dramatically (Figs. 7*A1,A2*). Just as blocking I_{Adepol} could affect the behavior of I_{K-V} via its effects on spike shape, blocking I_{K-V} likewise influenced I_{Adepol} waveforms. The increase in average spike duration during a train of spikes generated with I_{K-V} blocked resulted in cumulative inactivation of I_{Adepol} that was faster than that in control conditions (Fig. 7*B1,B2,B4*).

Next we investigated whether blocking inactivation of I_{K-V}

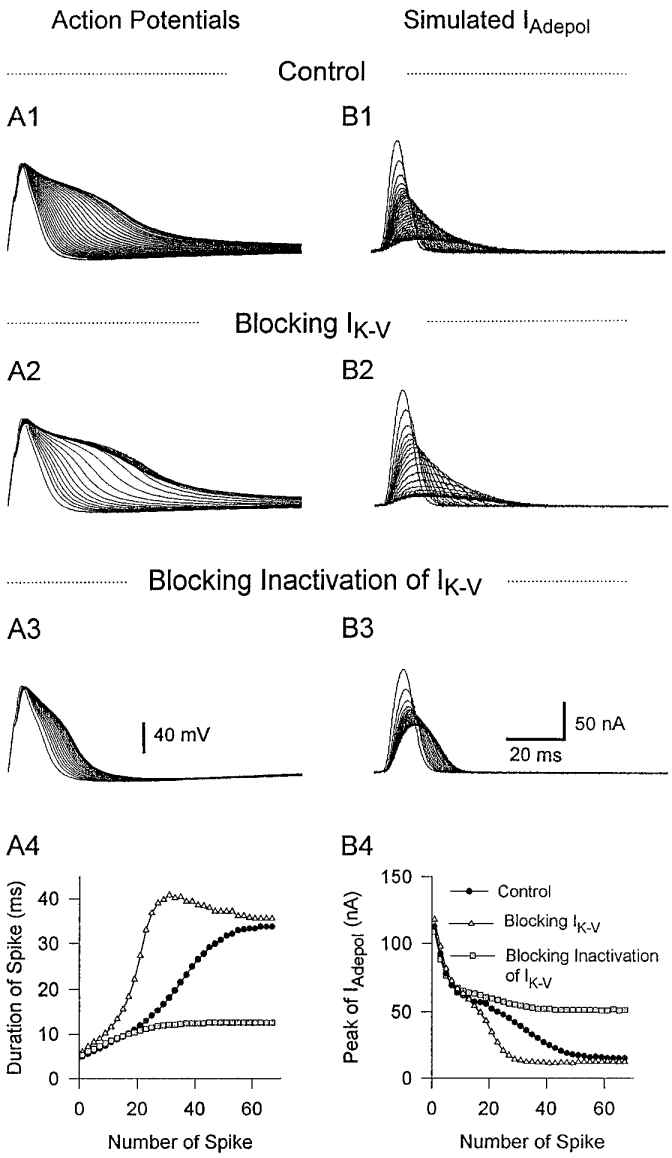

Figure 7. Blocking I_{K-V} activation (or inactivation) with the dynamic clamp accelerated (or reduced) spike broadening, which, in turn, modified the rate and extent of I_{Adepol} inactivation. *A*, Action-potential trains were evoked under control conditions (*A1*), after blocking I_{K-V} (*A2*), or after blocking inactivation of I_{K-V} (*A3*). The dynamic clamp was used in closed-loop mode either to simply cancel out I_{K-V} (*A2*) or to replace it with a noninactivating version of I_{K-V} (*A3*). *B*, Compared with control (*B1*), simulated I_{Adepol} underwent faster inactivation during a spike train with I_{K-V} blocked (*B2*) or slower and less complete inactivation with inactivation of I_{K-V} blocked (*B3*). *A4, B4*, Changes in spike width (*A1–A3*) and peak values of I_{Adepol} (*B1–B3*) caused by modifying I_{K-V} are plotted against spike number. Resting potential was −50 mV. G_{max} used by the dynamic clamp for blocking or modifying I_{K-V} was 1700 nS. G_{max} of I_{Adepol} used for simulating I_{Adepol} in *B1–B3* was 1950 nS.

would affect spike broadening during a train. The amplitude of I_{K-V} during a single spike is relatively small compared with I_{Adepol} (Fig. 2), and blocking it completely has no effect on the duration of a single spike (Fig. 7; Fig. 13 in Ma and Koester, 1995). One might therefore predict that eliminating its inactivation would have a negligible effect on spike broadening. On the contrary, blocking inactivation of I_{K-V} with the dynamic clamp reduced maximal spike broadening during a train by ~75% (Fig. 7*A1,A3,A4*). This ability of blocking I_{K-V} inactivation to limit

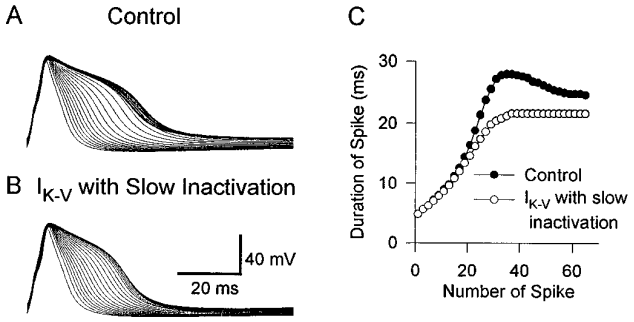

Figure 8. Replacing the rapid, state-dependent inactivation of I_{K-V} by a slower, Hodgkin–Huxley-type version reduced both the rate and final extent of spike broadening. *A*, An action-potential train was evoked by injecting brief depolarizing current pulses under control conditions. *B*, An action-potential train was evoked after eliminating the state-dependent inactivation of I_{K-V}, which was achieved by injecting two currents into the cell simultaneously: I_{K-V} with normal state-dependent inactivation but with reversed sign to block the existing I_{K-V} of the cell and I_{K-V} with only slow inactivation and normal polarity to replace the endogenous current. *C*, The durations of spikes for these two trains are plotted against the number of spike. Resting potential was −48 mV. G_{max} used by the dynamic clamp for blocking or modifying I_{K-V} was 2100 nS.

strongly the spike broadening can be explained as follows. Under normal conditions, I_{K-V} becomes a major component of repolarizing current in the early-to-middle portion of the train, because cumulative inactivation of I_{Adepol} causes longer spike durations, which in turn generate enhanced activation of I_{K-V}. Eventually, I_{K-V} amplitudes begin to decline later in the train, as cumulative I_{K-V} inactivation outstrips the increase in I_{K-V} activation (Figs. 2, 5*B*; Fig. 8 in Ma and Koester, 1995). As a result of the gradual rise and fall of I_{K-V} during the train, blocking its inactivation can add significantly to the repolarizing drive of the cell, thereby limiting the broadening process.

Simulation of I_{Adepol} waveforms with the dynamic clamp driven by the spike trains recorded with I_{K-V} in various different functional states revealed an important positive feedback interaction between inactivation of I_{Adepol} and spike broadening. There was a positive correlation between mean-spike duration during a train and rate of inactivation of simulated I_{Adepol} under three conditions: (1) inactivation of I_{K-V} blocked, (2) normal I_{K-V} and (3) activation of I_{K-V} blocked (Fig. 7*A4,B4*). Because I_{Adepol}-gating properties were not modified in this series of experiments, the three different patterns of its inactivation must be secondary to changes in action-potential waveforms caused by changing I_{K-V}. These data indicate that normally, as inactivation of I_{Adepol} during the course of a train contributes to spike broadening, the broadening in turn allows additional inactivation of I_{Adepol} to occur, thereby further enhancing broadening. Any other process that contributes to broadening, such as I_{K-V} inactivation, would be amplified by this positive feedback effect.

How would the balance between increasing activation and inactivation of I_{K-V} during a train be shifted if I_{K-V} did not undergo state dependent inactivation? This question was examined by comparing spike broadening under two conditions: (1) with native I_{K-V} inactivation kinetics, or (2) with the I_{K-V} conductance replaced by a modified version in which I_{K-V} inactivation parameters are fit by the current decay during a single, long voltage step, rather than by the state-dependent inactivation kinetics approximated from peak values of I_{K-V} measured during a train of brief steps (Fig. 4*A,B*). The nonstate-dependent value of τ_h is slower than the state-dependent version, and substituting it in the

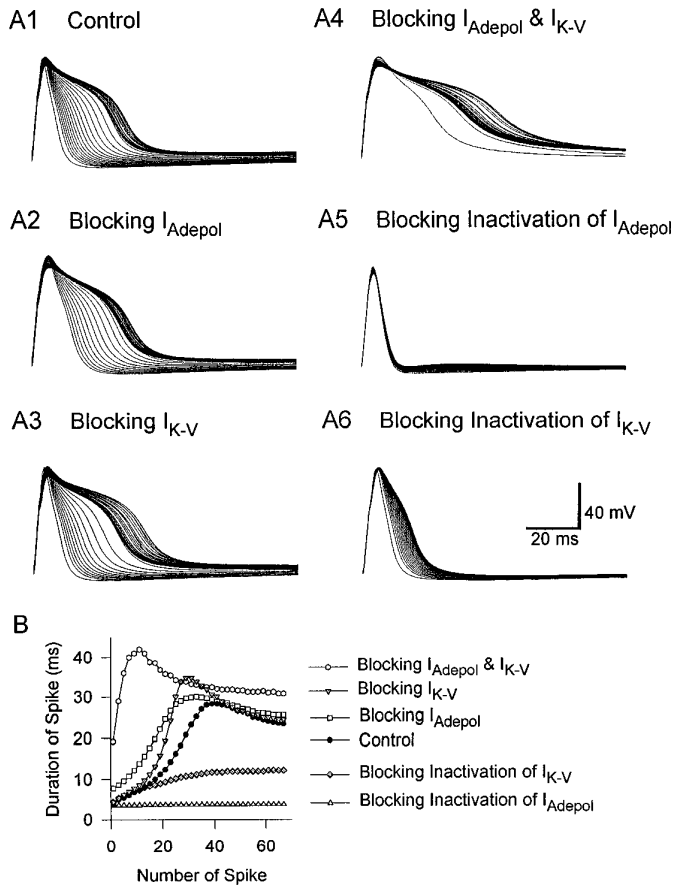

Figure 9. Using the dynamic clamp to block activation or inactivation of I_{Adepol} or of I_{K-V} caused changes in frequency-dependent spike broadening that were measured in the same cell. *A*, Action-potential trains generated with K^+ conductances in various different states. *A1*, Control; *A2*, with I_{Adepol} blocked; *A3*, with I_{K-V} blocked; *A4*, with I_{Adepol} and I_{K-V} blocked; *A5*, with inactivation of I_{Adepol} blocked; *A6*, with inactivation of I_{K-V} blocked. *B*, Durations of spikes in *A1–A6* are plotted against spike number. Resting potential was −50 mV. Currents were blocked or modified by using G_{max} for I_{Adepol} = 1750 nS and G_{max} for I_{K-V} = 1650 nS.

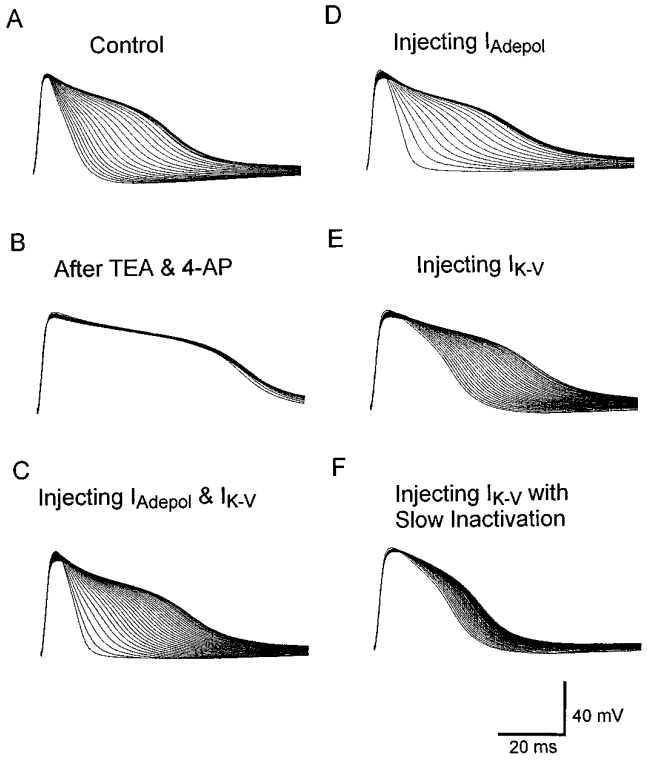

Figure 10. Addition of either I_{Adepol} or I_{K-V} with the dynamic clamp was sufficient to cause spike broadening in a cell in which K^+ currents had been preblocked pharmacologically. An action-potential train was evoked: *A*, In normal ASW. *B*, After 50 mM TEA and 10 mM 4-AP had been added to block I_{K-V}, I_{K-Ca}, and I_{Adepol}. *C*, With both I_{Adepol} and I_{K-V} added back. *D*, With I_{Adepol} added back. *E*, With I_{K-V} added back. *F*, With I_{K-V}, modified to express only the slow, nonstate-dependent inactivation, added back. Resting potential was −47 mV. G_{max} for I_{Adepol}, 1500 nS; G_{max} for I_{K-V}, 1500 nS (n = 6).

dynamic-clamp model of I_{K-V} limits cumulative inactivation of I_{K-V} and reduces by 22% (±1.4%; n = 4) the amount of spike broadening that occurs (Figs. 4*C5*, 8). Thus the enhanced inactivation resulting when depolarization is broken up into short pulses potentiates the rate and extent of broadening.

I_{Adepol} and I_{K-V} contribute differently to spike broadening

To compare the relative effects of I_{Adepol} and I_{K-V} on spike broadening directly, we used the dynamic clamp to block or to modify the two currents in the same cell. As described above, blocking I_{Adepol} caused a doubling in width of the first spike in the train (Fig. 9*A1,A2,B*). In contrast, blocking I_{K-V} had no effect on the width of the first spike but caused an acceleration of broadening in the first half of the train (Fig. 9*A1,A3,B*). When both I_{Adepol} and I_{K-V} were blocked simultaneously, the effects on spike width were variable. In most cells (9 of 14), the first spike in the train was not as wide as the maximally broadened spikes in a normal train (Fig. 9*A4,B*). As the train progressed, the spikes broadened significantly, presumably because of the transient decay of I_{K-Ca} (Fig. 6*B3*). Spike width then decayed as I_{K-Ca} facilitated, and I_{Ca} underwent progressive inactivation (compare Figs. 2 and 6). In other cells (5 of 14), the first spike in the train was broader than the widest spike in a normal train. In these cells, with both $I_{Adepol}$and I_{K-V} blocked, I_{K-Ca} cells have a limited ability to take over as the major repolarizing influence early in the train.

The relative effects of blocking inactivation of either I_{K-V} or I_{Adepol} also were examined in the same cell (n = 14). As expected from results described above (Figs. 5, 7), blocking inactivation of I_{Adepol} completely blocked broadening, whereas blocking inactivation of I_{K-V} blocked most, but not all, of the broadening (Fig. 9*A5,A6*). These results further support the hypothesis that cumulative inactivation of I_{Adepol} is essential for initiating spike broadening, and cumulative inactivation of I_{K-V} is essential to allow broadening to reach its full extent.

Simulated I_{Adepol} and I_{K-V} are sufficient to cause spike broadening

To test further our conclusions about the relative roles of I_{Adepol} and I_{K-V} in broadening, we blocked the entire complement of depolarization-activated K^+ currents pharmacologically and then added back I_{Adepol} and/or I_{K-V} with the dynamic clamp to see how they affected broadening. After first recording a control spike train, we blocked I_{Adepol}, I_{K-V}, and I_{K-Ca} by addition of 50 mM TEA and 10 mM 4-AP. With the outward currents blocked in this way, the first spike in the train was broadened maximally, and no significant change in spike duration occurred throughout the train (Fig. 10*A,B*). While maintaining the pharmacological block, I_{Adepol}, I_{K-V}, or the two together were added back to the

cell. Unlike the experiments described above, we did not measure the values of G_{max} for I_{Adepol} and $I_{K\text{-}V}$ in this set of experiments. Instead, the average G_{max} of both currents determined in earlier experiments was used as a starting point for the dynamic-clamp program (1700 nS for I_{Adepol} and 2100 nS for $I_{K\text{-}V}$). Then several different runs were made in which these initial values were bracketed by values of G_{max} that varied in steps of ±20%. We found that a wide range of G_{max} values for the two currents gave qualitatively similar results. The maximum value used was twice as large as the minimum value for both currents, i.e., G_{max} of I_{Adepol} ranged from 1300 to 2600 nS and G_{max} of $I_{K\text{-}V}$ ranged from 1500 to 3000 nS.

Adding back both I_{Adepol} and $I_{K\text{-}V}$ resulted in a spike train similar to that recorded under control conditions. The main difference was that, with $I_{K\text{-}Ca}$ still blocked by TEA, broadening at the end of the train, when $I_{K\text{-}Ca}$ normally has its maximal effect, was slightly greater than in the control (compare Fig. 10*A* and *C*). The incomplete inactivation of simulated I_{Adepol} at the end of a train (Fig. 3*C3*) seems to work against this extra broadening, as indicated by the fact that the protocol in Fig. 10*C* enhances broadening less than does blocking $I_{K\text{-}Ca}$ by BAPTA injection (Fig. 14*A1,A2* in Ma and Koester, 1995). Adding back I_{Adepol} alone resulted in a spike train in which the first spike had a normal duration, and broadening occurred much more rapidly than in the control condition (Fig. 10*A,D*), because the normally potentiating $I_{K\text{-}V}$ (Fig. 4*C2*) as well as $I_{K\text{-}Ca}$ still were blocked pharmacologically. Restoring $I_{K\text{-}V}$ alone resulted in a train in which the width of the first spike was threefold longer than the first control spike (Fig. 10*A,E*). This enhanced duration, with $I_{K\text{-}Ca}$ and I_{Adepol} blocked, is larger than that seen by blocking only I_{Adepol} (Figs. 5*A*, 6*A*), confirming the hypothesis that $I_{K\text{-}Ca}$ can play a significant role in repolarization of a single spike if I_{Adepol} is blocked (Fig. 6). If the $I_{K\text{-}V}$ that was added back had the slow time constant of inactivation measured from long pulses, rather than the state-dependent inactivation τ_h approximated by the brief pulse-train protocol, broadening was reduced (Fig. 10*F*). This difference between the results achieved with the Hodgkin–Huxley versus the state-dependent model of inactivation (see also Fig. 8) indicates that the relatively rapid state-dependent $I_{K\text{-}V}$ inactivation mechanism plays an important role in allowing inactivation of this current to build up during a spike train. Overall, the results obtained by adding back I_{Adepol} or $I_{K\text{-}V}$ with the dynamic clamp were consistent with those obtained with the complementary approach of blocking the currents with the dynamic clamp.

DISCUSSION

Application of the dynamic-clamp method to the R20 neurons

There were several technical limitations in this study. The space clamp was imperfect, as significant neuritic stumps remained connected to the soma. Using different concentrations of the same drug (TEA) to block either $I_{K\text{-}Ca}$ or $I_{K\text{-}V}$ quite likely resulted in a minor contamination of the difference currents obtained. The software used could not simulate two time constants for inactivation or recovery from inactivation (for I_{Adepol}) or state-dependent inactivation (for $I_{K\text{-}V}$), so these processes had to be approximated. The value of G_{max} used by the program had to be estimated for each individual cell from measurements made at the end of the experiment. Despite these limitations, the results obtained were highly consistent from preparation to preparation, and there was a high degree of internal consistency when results were compared from current-clamp, voltage-clamp, and dynamic-clamp protocols, in both this and the earlier study (Ma and Koester, 1995). All of these approaches provided data that fit a unified interpretation of spike broadening summarized in Figure 11.

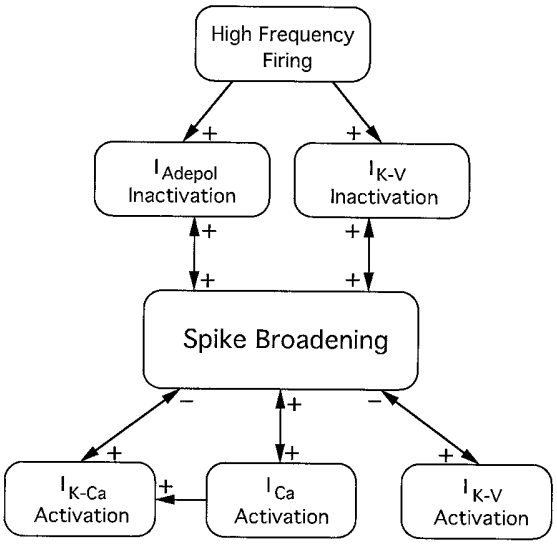

Figure 11. Summary of the predominant mechanisms underlying spike broadening in the R20 neurons, determined in this and the previous study (Ma and Koester, 1995). Some interactions that play a minor role in spike broadening are not included in this diagram. For example, spike broadening also facilitates the activation of I_{Adepol} (Fig. 3*C4*). This effect is overwhelmed by the progressive increase in inactivation, however. Broadening also enhances cumulative inactivation of I_{Ca} (Ma and Koester, 1995). This effect has two opposing effects on spike broadening: by reducing inward current it limits broadening, and by reducing the build-up of $I_{K\text{-}Ca}$, it enhances broadening.

Relative roles of I_{Adepol}, $I_{K\text{-}V}$, and $I_{K\text{-}Ca}$ in spike repolarization

Several lines of evidence indicate that I_{Adepol} is the major current responsible for repolarization of a single spike in the R20 cells. During the first spike in a train, I_{Adepol} is the largest and most rapidly activating of the three K^+ currents (Fig. 2). Moreover, with $I_{K\text{-}V}$ and $I_{K\text{-}Ca}$ blocked, I_{Adepol} is sufficient to cause normal repolarization of a single spike, but blocking all three K^+ currents caused ~10- to 15-fold spike broadening (Fig. 10*A,B*; Fig. 13 in Ma and Koester, 1995). Likewise, if $I_{K\text{-}V}$, $I_{K\text{-}Ca}$, and I_{Adepol} all are blocked pharmacologically, adding back I_{Adepol} with the dynamic clamp restores normal spike width (Fig. 10*A,B,D*). These results suggest that I_{Adepol} is the major current responsible for spike repolarization. However, blocking I_{Adepol} alone causes only a twofold increase in spike duration (Figs. 5*A*, 6*A*). The cause of this surprisingly small effect of blocking I_{Adepol} on spike width was revealed by simulating $I_{K\text{-}V}$ and measuring $I_{K\text{-}Ca}$ during the spike trains recorded with I_{Adepol} blocked. These data showed that $I_{K\text{-}V}$ amplitude is increased two- to threefold in response to twofold spike broadening, thereby allowing it to become a major repolarizing influence (Fig. 5*B2,B4*). This enhanced activation occurs because $I_{K\text{-}V}$ activation is slow compared with normal spike duration (compare Fig. 4*B* and *C*). $I_{K\text{-}Ca}$ also activates relatively slowly (Fig. 5 in Ma and Koester, 1995). It is potentiated 2.5- to fourfold by twofold spike broadening and likewise contributes to limiting spike broadening when I_{Adepol} is blocked (Fig. 6). These results illustrate how, in a system with several voltage-gated conductances, the effect produced by blocking a single current (e.g., I_{Adepol}) can underestimate significantly the physiological effect of

that current (cf. McCormick and Huguenard, 1992). In this case, blockade of I_{Adepol} is compensated largely by the emergence of two latent currents, $I_{K\text{-}V}$ and $I_{K\text{-}Ca}$.

Cumulative inactivation of I_{Adepol}, potentiated by a positive feedback interaction with spike broadening, is essential for initiation of broadening

Several lines of evidence confirm that I_{Adepol} inactivation is essential for spike broadening. (1) It is the largest outward current during the first spike in the train, but as the train progresses, it inactivates to 0–10% of its initial value (Figs. 2, 3*C2*, 7*B1*). (2) Changes in the other voltage-activated currents during the train are insufficient to explain broadening either qualitatively or quantitatively (Fig. 2; Ma and Koester, 1995). (3) Keeping spike width constant reduces only partially the progressive decrease in I_{Adepol} amplitudes during a train, indicating that a significant portion of its progressive inactivation is not secondary to broadening but, rather, acts as a primary cause of broadening (Fig. 12*D* in Ma and Koester, 1995). (4) When the other voltage-gated outward currents ($I_{K\text{-}V}$ and $I_{K\text{-}Ca}$) are blocked pharmacologically, either endogenous I_{Adepol} or simulated I_{Adepol} that is generated by the dynamic clamp can mediate frequency-dependent broadening (Fig. 10*D*; Fig. 14*A3* in Ma and Koester, 1995). (5) Blocking inactivation of I_{Adepol} completely eliminates frequency-dependent broadening (Figs. 5*A3*, 9*A5*).

Unlike other neurons in which the mechanisms of frequency-dependent spike broadening have been examined in detail (Aldrich et al., 1979a,b; Quattrocki et al., 1994), the progressive inactivation of the critical current in the R20 cells, I_{Adepol}, is not attributable primarily to state-dependent, cumulative inactivation. It has been proposed that the AKv1.1a gene product forms the ion channels for native I_{Adepol} measured in *Aplysia* neurons (Pfaffinger et al., 1991). Furukawa (1995) described pronounced state-dependent, cumulative inactivation of the AKv1.1a channels expressed in frog oocytes. When brief depolarizing pulses from a holding potential of −50 mV were repeated at 0.1 Hz, the evoked AKv1.1.a current pulses declined during the train in a manner that could be fit best by a kinetic model with state-dependent inactivation (Furukawa, 1995). We observed no such build-up of inactivation of I_{Adepol} in the R20 cells using the identical protocol. Higher frequency (7 Hz) trains of depolarizing voltage steps, designed to mimic the spike trains used in this study, did produce modest cumulative inactivation of I_{Adepol} from step to step in the R20 cells. However, this progressive inactivation could be simulated by the conventional Hodgkin–Huxley-type kinetic scheme described above without invoking state-dependent processes (data not shown). This difference in inactivation properties may indicate that the AKv1.1a gene product is not a component of the I_{Adepol} channels. More likely, given the other strong similarities between native I_{Adepol} and $I_{AKv1.1a}$ (Pfaffinger et al., 1991; Kaang et al., 1992), they differ in their inactivation properties either because of differences in ion composition or post-translational modification between oocytes and *Aplysia* neurons or because the AKv1.1a channels lack unidentified β-subunits or heterologous α-subunits that may be present in native I_{Adepol} channels (Sheng et al., 1993; Rettig et al., 1994).

The mechanism by which I_{Adepol} inactivation builds up during a train can be explained by the relation of I_{Adepol} channel kinetics to spike duration and interspike interval. Because of its rapid inactivation rate, significant, though not complete, inactivation of I_{Adepol} can occur during a single spike (Fig. 3*C5*). The time constant of recovery of I_{Adepol} from inactivation is on the order of 1 sec at −50 mV. Thus, for a 7 Hz train, a significant amount of inactivation that occurs during each spike will persist into the onset of the succeeding spike and beyond. Over the course of a 10 sec high-frequency train, one would expect the balance between inactivation and recovery from inactivation to reach an equilibrium within a few seconds if spike duration were constant (Fig. 12 in Ma and Koester, 1995); but empirically I_{Adepol} is found to continue to inactivate throughout the entire train if normal spike broadening is allowed to occur (Figs. 2, 3*C*). This extended inactivation occurs because spike broadening caused by persistent I_{Adepol} inactivation from previous spikes causes I_{Adepol} in succeeding spikes to undergo more complete inactivation, as h approaches more fully its steady-state value, h_∞. That is, there is positive feedback between inactivation and broadening. This coupling is illustrated by the positive correlation between spike width and the rate and extent of I_{Adepol} inactivation when spike width is manipulated artificially (Fig. 7; compare Figs. 7*C* and 12*D* in Ma and Koester, 1995). Broadening can also increase activation, which would provide a negative feedback force tending to resist broadening; because I_{Adepol} activates quickly with respect to spike rise time, increasing spike duration has only a relatively modest tendency to cause I_{Adepol} activation to facilitate. Enhanced inactivation is the predominant effect (Fig. 3*C5*).

Cumulative state-dependent inactivation of $I_{K\text{-}V}$, potentiated by a positive feedback interaction with spike broadening, is essential for maximum broadening

During a spike train, there is a constantly varying interplay between the changes in activation and inactivation of $I_{K\text{-}V}$. Early in the train there is a large scope for facilitation of $I_{K\text{-}V}$ in response to the spike broadening that is caused by I_{Adepol} inactivation, because $I_{K\text{-}V}$ activates so slowly relative to spike duration. As a result, $I_{K\text{-}V}$ increases during the first part of the train (Figs. 2, 4*C*), and blocking $I_{K\text{-}V}$ speeds up broadening (Figs. 7*A*, 9*B*; Fig. 14 in Ma and Koester, 1995). As spike width begins to approach its limit, $I_{K\text{-}V}$ approaches full activation, so the dominant effect of broadening on $I_{K\text{-}V}$ becomes to potentiate inactivation, which is a much slower process than activation. The importance of inactivation dynamics throughout the train is illustrated by the fact that cumulative inactivation contributes to limiting the amplitude of $I_{K\text{-}V}$ even as the $I_{K\text{-}V}$ peaks are increasing from spike to spike early in the train (Fig. 4*C6*). Thus, blocking inactivation of $I_{K\text{-}V}$ greatly reduces spike broadening (Figs. 7*A4*, 9*A6*).

As in the case of I_{Adepol}, there is a positive feedback interaction between spike broadening and inactivation of $I_{K\text{-}V}$. For simulated and recorded $I_{K\text{-}V}$, only a moderate cumulative inactivation occurs when spike broadening is prevented during a train. This inactivation is enhanced greatly when broadening is allowed to occur (Fig. 5*A4,B4*) (see Fig. 12 in Ma and Koester, 1995).

The state-dependent nature of $I_{K\text{-}V}$ inactivation, which causes it to be inactivated more effectively by brief pulses, is important in determining the role of $I_{K\text{-}V}$ in spike broadening. When native $I_{K\text{-}V}$ currents are substituted by $I_{K\text{-}V}$ currents with slower, nonstate-dependent inactivation kinetics, the rate of broadening is slower and less complete than the rate that occurs normally (Fig. 8). Moreover, after blocking all outward currents pharmacologically, adding back such a slowly inactivating current with the dynamic clamp is insufficient to restore significant frequency-dependent broadening (Fig. 10*F*). In contrast, the model that

approximated state-dependent inactivation kinetics generated robust frequency-dependent broadening (Fig. 10*E*).

Summary and conclusions

The major interactions between currents and membrane potential that determine the dynamics of frequency-dependent spike broadening are summarized in Figure 11. During the first action potential in a train, I_{Adepol} activates relatively rapidly and therefore dominates the repolarization process. However, the inactivation that occurs during each spike accumulates from spike to spike, causing progressive broadening. In addition, because inactivation of I_{Adepol} is relatively slow with respect to spike duration, the broadening has a positive feedback effect on I_{Adepol} inactivation. $I_{K\text{-}V}$ and $I_{K\text{-}Ca}$ are latent currents that have no significant effect on repolarization during the first spike in the train. The broadening also allows $I_{K\text{-}V}$ and $I_{K\text{-}Ca}$, which activate relatively slowly, to turn on more fully during successive spikes in the train, thereby playing a greater role in repolarization. The broader spikes also prolong I_{Ca}. This added Ca^{2+} influx, on the one hand, supports the shoulders of the broadened spikes but, on the other hand, limits spike broadening by elevating cytoplasmic Ca^{2+}, which potentiates $I_{K\text{-}Ca}$. As the train progresses, the enhanced $I_{K\text{-}V}$ activation caused by broadening gradually is overwhelmed by progressive build-up of $I_{K\text{-}V}$ inactivation, which is amplified by a positive feedback relation between broadening and inactivation. As a result of these complex dynamics, control of repolarization gradually devolves from I_{Adepol} to $I_{K\text{-}V}$ to $I_{K\text{-}Ca}$ during the course of a high-frequency spike train.

REFERENCES

Aldrich RW (1981) Inactivation of voltage-gated delayed potassium current in molluscan neurons: a kinetic model. Biophys J 36:519–532.

Aldrich RW, Getting PA, Thompson SH (1979a) Inactivation of delayed outward current in molluscan neurone somata. J Physiol (Lond) 291:507–530.

Aldrich RW, Getting PA, Thompson SH (1979b) Mechanism of frequency-dependent broadening of molluscan neurone soma spikes. J Physiol (Lond) 291:531–544.

Alevizos A, Weiss KR, Koester J (1989) SCP-containing R20 neurons modulate respiratory pumping in *Aplysia.* J Neurosci 9:3058–3071.

Baukrowitz T, Yellen G (1995) Modulation of K^+ current by frequency and external $[K^+]$: a tale of two inactivation mechanisms. Neuron 15:951–960.

Bielefeldt K, Rotter JL, Jackson MB (1992) Three potassium channels in rat posterior pituitary nerve terminals. J Physiol (Lond) 458:41–67.

Byrne JH (1980a) Analysis of ionic conductance mechanisms in motor cells mediating inking behavior in *Aplysia californica.* J Neurophysiol 43:630–650.

Byrne JH (1980b) Quantitative aspects of ionic conductance mechanisms contributing to firing pattern of motor cells mediating inking behavior in *Aplysia californica.* J Neurophysiol 43:651–668.

Byrne JH, Shapiro E, Dieringer N, Koester J (1979) Biophysical mechanisms contributing to inking behavior in *Aplysia*. J Neurophysiol 42:1233–1250.

Coates CJ, Bulloch AG (1985) Synaptic plasticity in the molluscan peripheral nervous system: physiology and role for peptides. J Neurosci 5:2677–2684.

Crest M, Gola M (1993) Large conductance Ca^{2+}-activated K^+ channels are involved in both spike shaping and firing regulation in *Helix* neurons. J Physiol (Lond) 465:265–287.

De Schutter E, Bower JM (1994) An active membrane model of the cerebellar purkinje cell. I. Simulation of current clamps in slice. J Neurophysiol 70:375–399.

Ducreux C, Puizillout J-J (1995) A-current modifies the spike of C-type neurons in the rabbit nodose ganglion. J Physiol (Lond) 486:439–451.

Furukawa Y (1995) Accumulation of inactivation in a cloned transient K^+ channel (AKv1.1a) of *Aplysia*. J Neurophysiol 14:1248–1257.

Furukawa Y, Kandel ER, Pfaffinger P (1992) Three types of early transient potassium currents in *Aplysia* neurons. J Neurosci 12:989–1000.

Gillette R, Gillette MU, Davis WJ (1980) Substrates of command ability in a buccal neuron of *Pleurobranchaea.* I. Mechanisms of action potential broadening. J Neurophysiol 43:669–685.

Golowasch J, Buchholtz F, Epstein IR, Marder E (1992) Contribution of individual ionic currents to activity of a model stomatogastric ganglion neuron. J Neurophysiol 67:341–349.

Hermann A, Gorman ALF (1981a) Effects of 4-aminopyridine on potassium currents in a molluscan neuron. J Gen Physiol 78:63–86.

Hermann A, Gorman ALF (1981b) Effects of tetraethylammonium on potassium currents in a molluscan neuron. J Gen Physiol 78:87–110.

Hodgkin AL, Huxley AF (1952) A quantitative description of membrane current and its application to conduction and excitation in nerve. J Physiol (Lond) 117:500–544.

Jackson MB, Konnerth A, Augustine GJ (1991) Action potential broadening and frequency-dependent facilitation of calcium signals in pituitary nerve terminals. Proc Natl Acad Sci USA 88:380–384.

Kaang BK, Pfaffinger PJ, Grant SGN, Kandel ER, Furukawa Y (1992) Overexpression of an *Aplysia* Shaker K^+ channel gene modifies the electrical properties and synaptic efficacy of identified *Aplysia* neurons. Proc Natl Acad Sci USA 89:1133–1137.

Ma M, Koester J (1995) Consequences and mechanisms of spike broadening of the R20 cells in *Aplysia californica.* J Neurosci 15:6720–6734.

Marom S, Levitan IB (1994) State-dependent inactivation of the KV3 potassium channel. Biophys J 67:579–589.

McCormick DA, Huguenard JR (1992) A model of electrophysiological properties of thalamocortical relay neurons. J Neurophysiol 68:1384–1400.

Pfaffinger PJ, Furukawa Y, Zhao B, Dugan D, Kandel ER (1991) Cloning and expression of an *Aplysia* K^+ channel and comparison with native *Aplysia* K^+ currents. J Neurosci 11:918–927.

Quattrocki EA, Marshall J, Kaczmarek LK (1994) A *Shab* potassium channel contributes to action potential broadening in peptidergic neurons. Neuron 12:73–86.

Rettig J, Heinemann SH, Wunder F, Lorra C, Parcej DN, Dolly JO, Pongs O (1994) Inactivation properties of voltage-gated K^+ channels altered by presence of β-subunit. Nature 369:289–294.

Schwindt PC (1992) Ionic currents governing input–output relations in Betz cells. In: single neuron computation (McKenna T, Davis J, Zornetzer SF, eds), pp. 235–258. New York: Academic.

Sharp AA, O'Neil MB, Abbott LF, Marder E (1993a) Dynamic clamp: computer-generated conductances in real neurons. J Neurophysiol 69:992–995.

Sharp AA, O'Neil MB, Abbott LF, Marder E (1993b) The dynamic clamp: artificial conductances in biological neurons. Trends Neurosci 16:389–394.

Sheng M, Liao YJ, Jan YN, Jan LY (1993) Presynaptic A-curent based on heteromultimeric K^+ channels *in vivo.* Nature 365:72–75.

Tierney AJ, Harris-Warrick RM (1992) Physiological role of the transient potassium current in the pyloric circuit of the lobster stomatogastric ganglion. J Neurophysiol 67:599–609.